Velocity and Position Control of a Wheeled Inverted Pendulum by Partial Feedback Linearization

Kaustubh Pathak, Jaume Franch, and Sunil K. Agrawal

Abstract—In this paper, the dynamic model of a wheeled inverted pendulum (e.g., Segway, Quasimoro, and Joe) is analyzed from a controllability and feedback linearizability point of view. First, a dynamic model of this underactuated system is derived with respect to the wheel motor torques as inputs while taking the nonholonomic no-slip constraints into considerations. This model is compared with the previous models derived for similar systems. The strong accessibility condition is checked and the maximum relative degree of the system is found. Based on this result, a partial feedback linearization of the system is obtained and the internal dynamics equations are isolated. The resulting equations are then used to design two novel controllers. The first one is a two-level velocity controller for tracking vehicle orientation and heading speed set-points, while controlling the vehicle pitch (pendulum angle from the vertical) within a specified range. The second controller is also a two-level controller which stabilizes the vehicle's position to the desired point, while again keeping the pitch bounded between specified limits. Simulation results are provided to show the efficacy of the controllers using realistic data.

Index Terms—Lyapunov methods, mobile robots, modeling, nonlinear systems, position control, velocity control.

I. INTRODUCTION

Mobile wheeled inverted pendulum models have evoked a lot of interest recently ([5], [3], [8], [6], [4], [14]) and at least one commercial product (Segway) is available [7]. Such vehicles are of interest because they have a small footprint and can turn on a dime. The kinematic model of the system is insufficient to describe the system behavior and has been proved to be uncontrollable [3]. In fact, balancing of the wheeled pendulum system is only achieved by considering dynamic effects.

Similar systems like the cart and pendulum, and the Pendubot [13] have been studied in the literature. Unlike these systems, however, the pendulum's motion in the present system is not planar and the motors driving the wheels are directly mounted on the pendulum body.

In an earlier work [5], a trajectory-tracking algorithm was found using a linear state-space model. A recent effort [6] concentrates on dynamic modeling and model identification. However, no control laws were derived. In Grasser *et al.* [8], a dynamic model was derived using a Newtonian approach and the equations were linearized around an operating point to design a controller. In Salerno *et al.* [3], the dynamic equations were studied, with the pendulum pitch and the rotation angles of the two wheels as the variables of interest. Various controllability properties of the system in terms of the state variables were analyzed using a differential-geometric approach. In a recent letter [4], Salerno *et al.* also design a linear controller for stabilization and study its robustness. A planar model without considering vehicle yaw, and a linear stabilizing controller was derived in [14].

In contrast, in this study, the dynamic modeling is done directly in terms of variables which are of interest with respect to the planning and
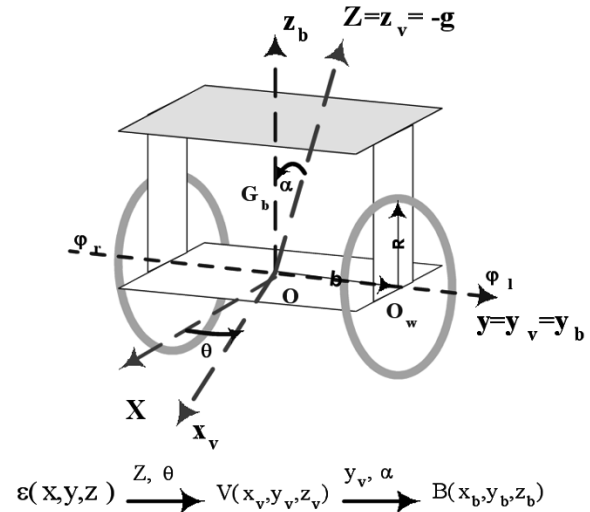
Fig. 1. Geometric parameters and coordinate systems for the system.

control of vehicle's position and orientation. A Lagrangian approach is used to derive the equations and the nonoholonomic constraint forces are eliminated. The equations are then simplified, reduced in order, and then checked for the strong-accessibility condition. It has been proved in this study, using a result from [1], that the maximum relative degree possible for the system is 4. A set of outputs is then chosen with the correct total relative degree and the system is put in the normal form [9] with the internal dynamics singled out. In Section V, a two-level controller is designed which makes use of the partial feedback linearization results. The controller keeps the vehicle pitch angle, i.e., the pendulum angle from the vertical, within specified limits and tracks the given orientation and heading-speed set-points which are assumed to be coming from a higher level controller for motion planning. In Section VI, another two-level controller is designed which is able to stabilize the vehicle to a point from any initial configuration and speeds while keeping the vehicle pitch bounded within specified limits.

II. DYNAMIC MODEL

Referring to Fig. 1, b is distance OO_w, where O is the point midway between the two wheel centers. R is the radius of both wheels. The pendulum body parameters have the subscript b, and the wheel parameters have subscript w. $\mathcal{E}(\mathbf{X}, \mathbf{Y}, \mathbf{Z})$ is an inertial frame. $\mathcal{B}(\mathbf{x_b}, \mathbf{y_b} = \mathbf{y}, \mathbf{z_b})$ is a frame attached to the pendulum body. $\mathcal{V}(\mathbf{x_v}, \mathbf{y_v} = \mathbf{y}, \mathbf{z_v} = \mathbf{Z})$ are the vehicle-fixed coordinates. The pitch angle α is $\angle(\mathbf{Z}, \mathbf{z_b})$, and the vehicle orientation angle θ equals $\angle(\mathbf{X}, \mathbf{x_v})$. The center of mass of the pendulum body G_b is at coordinates $OG_b = (c_x, 0, c_z)$ in $\mathcal{B}$. c_x would later be taken as 0 to simplify equations. M_b is the mass of the pendulum body, and

$$I_{b/\mathcal{B}} = \begin{pmatrix} I_{xx} & -I_{xy} & -I_{xz} \\ -I_{xy} & I_{yy} & -I_{yz} \\ -I_{xz} & -I_{yz} & I_{zz} \end{pmatrix}, \quad I_{xy} = 0, \quad I_{yz} = 0$$

is the inertia matrix of the pendulum body about its center of mass G_b in the basis $(\mathbf{x_b}, \mathbf{y_b}, \mathbf{z_b})$. $I_{xz} = 0$ if we take $c_x = 0$ and assume that the body is symmetric about the $\mathbf{x_b}$ axis. $[I_{wa}, I_{wd}]$ are the moment of inertia of a wheel about its axis and about a diameter respectively and M_w is its mass. ϕ_r and ϕ_l are the angles of rotation of the right and left wheels, respectively. The position vector of point O in $\mathcal{E}$ is (x_o, y_o, R).

The *rotational* kinetic energy of the pendulum body T_b^R and its *translational* kinetic energy are computed as

$$2T_b^R = \mathbf{\Omega}_{B/\mathcal{E}}^T I_{b/B} \mathbf{\Omega}_{B/\mathcal{E}}, \quad 2T_B^T = M_b \mathbf{v}_{\mathbf{G_b}/\mathcal{E}} \cdot \mathbf{v}_{\mathbf{G_b}/\mathcal{E}}. \quad (1)$$

The gravitational potential energy of the system is

$$U_B = M_b g(R + c_z \cos(\alpha)). \quad (2)$$

The rotational and translational kinetic energy due to the two wheels can be given by

$$2T_w^R = I_{wa}\dot{\phi}_r^2 + I_{wa}\dot{\phi}_l^2 + 2I_{wd}\dot{\theta}^2, \quad 2T_w^T = M_w R^2 \left(\dot{\phi}_r^2 + \dot{\phi}_l^2\right). \quad (3)$$

The configuration variables of the system are initially taken as

$$\mathbf{q}_{6 \times 1} = [x_o, y_o, \theta, \alpha, \phi_r, \phi_l]^T. \quad (4)$$

The motor-rotor inertial quantities are considered to be negligible compared to those of the wheels. The Lagrangian is therefore $L(\mathbf{q}) = T_B^T + T_b^R + T_w^R + T_w^T - U_B$. Using the Euler–Lagrange equations, the equations of motion can then be derived as

$$M(\mathbf{q})\ddot{\mathbf{q}} + V(\mathbf{q}, \dot{\mathbf{q}}) = E(\mathbf{q})\boldsymbol{\tau} + A^T(\mathbf{q})\boldsymbol{\lambda} \quad (5)$$

where $A(\mathbf{q})$ is the nonholonomic constraints matrix derived in the next section. $\boldsymbol{\tau}$ is the input motor-torque vector given by

$$\boldsymbol{\tau} = \begin{pmatrix} \tau_r \\ \tau_l \end{pmatrix}, \quad E(\mathbf{q}) = \begin{pmatrix} 0 & 0 \\ 0 & 0 \\ 0 & 0 \\ -1 & -1 \\ 1 & 0 \\ 0 & 1 \end{pmatrix}. \quad (6)$$

Note the structure of the fourth row of $E(\mathbf{q})$ which arises because the motors are mounted on the pendulum body. $\boldsymbol{\lambda}$ is the constraint-force vector.

The three nonholonomic constraints due to no-slip can be written as $A(\mathbf{q})_{3 \times 6}\dot{\mathbf{q}} = 0$, where

$$A(\mathbf{q})_{3 \times 6} = \begin{pmatrix} -\sin(\theta) & \cos(\theta) & 0 & 0 & 0 & 0 \\ \cos(\theta) & \sin(\theta) & b & 0 & -R & 0 \\ \cos(\theta) & \sin(\theta) & -b & 0 & 0 & -R \end{pmatrix}. \quad (7)$$

The null-space of $A(\mathbf{q})$ is given by the matrix $S(\mathbf{q})$ as

$$S(\mathbf{q})_{6 \times 3} = \begin{pmatrix} 0 & \cos(\theta) & 0 \\ 0 & \sin(\theta) & 0 \\ 0 & 0 & 1 \\ 1 & 0 & 0 \\ 0 & 1/R & b/R \\ 0 & 1/R & -b/R \end{pmatrix}. \quad (8)$$

The vector $\dot{\mathbf{q}}$ has to lie in this null-space, therefore

$$\dot{\mathbf{q}} = S(\mathbf{q})\boldsymbol{\nu}_{3 \times 1} \quad (9)$$
$$\boldsymbol{\nu} = [\dot{\alpha}, v, \dot{\theta}]^T \quad (10)$$

where v is the forward heading speed of the vehicle in the direction $\mathbf{x_v}$.

Next, we follow the standard procedure for the elimination of Lagrange multipliers λ by premultiplication with S^T to obtain

$$(S^T M S)\dot{\boldsymbol{\nu}} + S^T(M\dot{S}\nu + V(\mathbf{q}, \dot{\mathbf{q}})) = S^T E(\mathbf{q})\boldsymbol{\tau}. \quad (11)$$

We note that ϕ_r, ϕ_l are decoupled entirely from the rest of the state variables and $\dot{\phi}_r, \dot{\phi}_l$ can be found uniquely given $v, \dot{\theta}$ from (9). From a control point of view, we are not interested in these variables and can thus reduce the order of the system by 2.

We now define the configuration vector ($\mathbf{q_r}$) and the state vector ($\mathbf{x}$) as follows:

$$\mathbf{q_r} = [x_o, y_o, \theta, \alpha]^T, \quad \mathbf{x} = \begin{pmatrix} \mathbf{q_r} \\ \boldsymbol{\nu} \end{pmatrix}_{7 \times 1}. \quad (12)$$

This results in the last two rows of the $S(\mathbf{q})$ being removed, and we get a truncated matrix $S_r(\mathbf{q_r})_{4 \times 2}$. Another simplification can be obtained by assuming that the body is symmetric about the $\mathbf{x_b}$ axis. This implies that $I_{xz} = 0$ and $c_x = 0$. The input-affine form is then given by

$$\dot{\mathbf{x}} = \mathbf{f}(\mathbf{x}) + \mathbf{g}(\mathbf{x})\mathbf{u}$$
$$\mathbf{g}(\mathbf{x}) = \begin{pmatrix} \mathbf{0}_{4 \times 2} \\ (S^T M S)^{-1} S^T E \end{pmatrix}_{7 \times 2}, \quad \mathbf{u} = \begin{pmatrix} \tau_r \\ \tau_l \end{pmatrix}$$
$$\mathbf{f}(\mathbf{x}) = \begin{pmatrix} S_r \boldsymbol{\nu} \\ -(S^T M S)^{-1} S^T(M\dot{S}\boldsymbol{\nu} + V(\mathbf{q_r}, \dot{\mathbf{q}}_r)) \end{pmatrix}. \quad (13)$$

We partition $\mathbf{g}(\mathbf{x})$ and $\mathbf{f}(\mathbf{x})$ in the following way for future derivations:

$$\mathbf{g}(\mathbf{x})_{7 \times 2} = [\mathbf{g_1}(\mathbf{x}), \mathbf{g_2}(\mathbf{x})], \quad \mathbf{f}(\mathbf{x}) = \begin{pmatrix} \mathbf{f_1}(\mathbf{x}) \\ \mathbf{f_2}(\mathbf{x}) \end{pmatrix} \quad (14)$$
$$\mathbf{f_1}(\mathbf{x}) = \begin{pmatrix} \cos(\theta)v & \sin(\theta)v & \dot{\theta} & \dot{\alpha} \end{pmatrix}^T. \quad (15)$$

The detailed expressions for $\mathbf{g}(\mathbf{x})$ and $\mathbf{f_2}(\mathbf{x})$ have been provided in the Appendix.

III. STRONG ACCESSIBILITY CONDITION AND MAXIMUM RELATIVE DEGREE

This section is devoted to study of the strong accessibility condition and the feedback linearization of the system, either full or partial. The strong accessibility condition [2] is defined as follows.

Defining

$$\mathcal{C} = \langle\{[X_k, [X_{k-1}, [\dots, [X_1, g_j]\dots]]],$$
$$X_i \in \{f, g_1, \dots, g_m\}, j = 1, \dots, m, k \geq 1\}\rangle \quad (16)$$

where the notation $\langle\cdots\rangle$ denotes a distribution. If the dimension of $\mathcal{C}$ is n, then the system

$$\dot{x} = f(x) + \sum_{j=1}^{m} g_j(x)u_j \qquad x \in R^n \quad (17)$$

is *strongly accessible*.

Regarding the *largest feedback linearizable subsystem*, we refer to the construction in [1]. Consider the following sets and distributions:

$$G_0 = \langle g_1, \dots, g_m \rangle, \quad G_f = \{f + g, g \in G_0\} \quad (18)$$
$$G_i = \langle G_{i-1}, \{[G_f, G_{i-1}]\}\rangle, \quad Q_i = \left\langle \left\{ ad_f^i G_0, \overline{G}_{i-1} \right\} \right\rangle \quad (19)$$

where $[G_f, G_{i-1}] = \{[X, Y], \forall X \in G_f, Y \in G_{i-1}\}$, $\overline{G}_{i-1}$ means the involutive closure of G_{i-1}, $ad_f^i g = [f, ad_f^{i-1}g]$, while $ad_f^1 g = [f, g]$. Based on these definitions, compute the following integers:

$$r_0 = \dim G_0 \quad (20)$$
$$r_i = \dim Q_i - \dim \overline{G}_{i-1}, \quad \forall i \geq 1 \quad (21)$$
$$K_j = \#\{r_i \geq j, \forall i \geq 0\}, \quad j \geq 1. \quad (22)$$

Then, it follows that $r_1 \geq r_2 \geq \cdots$ and the maximum relative degree that one can achieve for the system (17) is $r_1 + r_2 + \cdots \leq n$.

Before computing these distributions and integers for f, g_1, g_2 given in the last section and the Appendix, we will apply a feedback law in order to simplify the input vector fields as much as possible. Since the fifth and sixth coordinates of g_1 and g_2 are equal, while the seventh is the same but with a different sign, we suggest the feedback law

$$v_1 = \frac{(u_1 + u_2)}{D_\alpha}, \quad v_2 = \frac{(u_1 - u_2)Rb}{G_\alpha}. \quad (23)$$

Here, G_α and D_α are as defined in the Appendix. Therefore, the new input vector fields are (we use the same notation for the new input vector fields)

$$g_1 = (0 \quad 0 \quad 0 \quad 0 \quad g_1[5] \quad g_1[6] \quad 0)^T \qquad (24)$$
$$g_2 = (0 \quad 0 \quad 0 \quad 0 \quad 0 \quad 0 \quad 1)^T \qquad (25)$$

where

$$g_1[5] = M_b R^2 + 2 M_w R^2 + 2 I_{\text{wa}} + M_b \cos(x_4) c_z R \qquad (26)$$
$$g_1[6] = -R \left(M_b \cos(x_4) c_z R + I_{yy} + M_b c_z^2 \right). \qquad (27)$$

Clearly, $G_0 = \langle g_1, g_2 \rangle$ has dimension 2. It is a straightforward computation to see $[g_1, g_2] = 0$, from where we infer that G_0 is involutive or, equivalently, $G_0 = \overline{G}_0$. This involutivity property is useful to see the equality

$$G_1 = \langle G_0, \{[G_f, G_0]\} \rangle = \langle G_0, [f, G_0] \rangle.$$

After Lie bracket computations, we have

$$G_1 = \langle g_1, g_2, [f, g_1], [f, g_2] \rangle \qquad (28)$$

where

$$[f, g_1] = (\alpha_1 \quad \alpha_2 \quad 0 \quad \alpha_4 \quad \alpha_5 \quad \alpha_6 \quad \alpha_7)^T$$
$$[f, g_2] = (0 \quad 0 \quad \beta_3 \quad 0 \quad \beta_5 \quad \beta_6 \quad \beta_7)^T$$

where α_i and β_j are certain nonzero functions that depend on the state variables. This distribution is not involutive since

$$[g_1, [f, g_1]] = (0 \quad 0 \quad 0 \quad 0 \quad \gamma_5 \quad \gamma_6 \quad 0)^T$$

where γ_5, γ_6 are functions depending on the state variables. Let us remark that the dimension of $\langle g_1, [g_1, [f, g_1]] \rangle = 2$. This is the reason why $[g_1, [f, g_1]] \notin G_1$. Hence

$$\overline{G}_1 \supset \tilde{G}_1 = \langle g_1, g_2, [f, g_1], [f, g_2], [g_1, [f, g_1]] \rangle$$
$$= \langle [f, g_1], \eta_3, \eta_5, \eta_6, \eta_7 \rangle \qquad (29)$$

where

$$\eta_3 = \begin{pmatrix} 0 \\ 0 \\ 1 \\ 0 \\ 0 \\ 0 \\ 0 \end{pmatrix}, \quad \eta_5 = \begin{pmatrix} 0 \\ 0 \\ 0 \\ 0 \\ 1 \\ 0 \\ 0 \end{pmatrix}, \quad \eta_6 = \begin{pmatrix} 0 \\ 0 \\ 0 \\ 0 \\ 0 \\ 1 \\ 0 \end{pmatrix}, \quad \eta_7 = \begin{pmatrix} 0 \\ 0 \\ 0 \\ 0 \\ 0 \\ 0 \\ 1 \end{pmatrix}. \qquad (30)$$

$\tilde{G}_1$ is still not involutive since $[\eta_3, [f, g_1]] \notin \tilde{G}_1$. Therefore

$$\overline{G}_1 \supset \langle \eta_3, \eta_5, \eta_6, \eta_7, [f, g_1], [\eta_3, [f, g_1]] \rangle.$$

It can be seen that the distribution on the right-hand side is not involutive because $[\eta_3, [\eta_3, [f, g_1]]]$ is not in that distribution. Therefore

$$\overline{G}_1 \supset \langle \eta_3, \eta_5, \eta_6, \eta_7, [f, g_1], [\eta_3, [f, g_1]], [\eta_3, [\eta_3, [f, g_1]]] \rangle = \Re^7.$$

This implies that $\overline{G}_1 = \Re^7$. Since $\overline{G}_1 \subset \mathcal{C} \subset \Re^7$, it follows that $\mathcal{C} = \Re^7$ and, hence, the system is strongly accessible.

On the other hand

$$Q_1 = \langle [f, G_0], G_0 \rangle = G_1$$

has dimension 4. Therefore, the integers $r_i, i \geq 0$ in (20) and (21) are

$$r_0 = \dim G_0 = 2$$
$$r_1 = \dim Q_1 - \dim \overline{G}_0 = 4 - 2 = 2$$
$$r_2 = \dim Q_2 - \dim \overline{G}_1 = 0. \qquad (31)$$

There is no need to compute more of these integers since they are positive and nonincreasing. Finally, the controllability indices $K_j, j \geq 1$ in (22) are $K_1 = \#\{r_i \geq 1, \forall i \geq 0\} = 2, K_2 = \#\{r_i \geq 2, \forall i \geq 0\} = 2, K_3 = \#\{r_i \geq 3, \forall i \geq 0\} = 0$. As before, there is no need to compute more of these indices because successive ones vanish. Summarizing, the largest feedback linearizable subsystem for the system has dimension 4.

IV. PARTIAL FEEDBACK LINEARIZATION

In this section, we partially feedback-linearize the system. Using a feedback law and a change of variables, we write the system as two chains of integrators, one for each input, plus three nonlinear equations which represents the internal dynamics of the system. By definition [9], the inputs do not appear explicitly in the internal dynamics equations.

We shall find two variables whose relative degrees together match the maximum relative degree found in the previous section. Later on, three new variables ϕ_1, ϕ_2, ϕ_3 will be obtained such that they are independent of the variables, whose relative degree is two, and their derivatives.

It is not difficult to see that both $x_3 = \theta$ and $x_4 = \alpha$ have relative degree 2. Their equations are

$$\dot{x}_3 = x_7, \quad \dot{x}_7 = f_2[3] + v_2$$
$$\dot{x}_4 = x_5, \quad \dot{x}_5 = f_2[1] + g_1[5] v_1. \qquad (32)$$

In order to convert (32) into two chains of integrators, a new feedback law is applied

$$w_1 = f_2[3] + v_2 \qquad (33)$$
$$w_2 = f_2[1] + g_1[5] v_1. \qquad (34)$$

After this feedback law, the input-vector fields become

$$G_m = (\bar{g}_1 \quad \bar{g}_2)$$
$$\bar{g}_1(\mathbf{x}) = (0 \quad 0 \quad 0 \quad 0 \quad 0 \quad 0 \quad 1)^T$$
$$\bar{g}_2(\mathbf{x}) = (0 \quad 0 \quad 0 \quad 0 \quad 1 \quad g_1[6]/g_1[5] \quad 0)^T \qquad (35)$$

and the drift vector field becomes

$$\bar{\mathbf{f}}(\mathbf{x}) = \begin{pmatrix} x_6 \cos(x_3) \\ x_6 \sin(x_3) \\ x_7 \\ x_5 \\ 0 \\ f_2[2] - (g_1[6]/g_1[5]) f_2[1] \\ 0 \end{pmatrix} \qquad (36)$$

where the terms $f_2[1], f_2[2], f_2[3]$ are as defined in the Appendix. For the operational range of $\alpha \in (-\pi/2, \pi/2)$, $g_1[5] > 0$ unconditionally.

In order to obtain the three remaining coordinates of the change of variables, the condition

$$\nabla\phi_i G_m = \mathbf{0}, \quad i = 1, 2, 3 \tag{37}$$

must be fulfilled. Moreover, the gradients of ϕ_1, ϕ_2, ϕ_3 must be linearly independent of the gradients of the coordinates already chosen (x_3, x_7, x_4, x_5). Let us write $\nabla\phi_i = (a_1, a_2, a_3, a_4, a_5, a_6, a_7)$. The orthogonality condition (37) implies

$$a_7 = 0, \quad a_5 g_1[5] + a_6 g_1[6] = 0. \tag{38}$$

Equation (38) is satisfied if one takes

$$a_5 = -\lambda g_1[6], \quad a_6 = \lambda g_1[5] \tag{39}$$

for some nonzero λ which could be in general a function of $\mathbf{x}$.

Note that the terms $g_1[5], g_1[6]$ are functions of x_4 only. For integrability, the following conditions must be also satisfied:

$$\frac{\partial a_4}{\partial x_5} = \frac{\partial a_5}{\partial x_4} = -\lambda \frac{\partial g_1[6]}{\partial x_4}, \quad \frac{\partial a_4}{\partial x_6} = \frac{\partial a_6}{\partial x_4} = \lambda \frac{\partial g_1[5]}{\partial x_4} \tag{40}$$

while a_1, a_2, a_3 can be chosen as desired. Therefore, one feasible choice for the remaining coordinates is

$$\phi_1 = x_1, \quad \phi_2 = x_2, \quad \phi_3 = -x_5 g_1[6] + x_6 g_1[5]. \tag{41}$$

All of the these can be verified to satisfy (38) and (40). Summarizing, the change of coordinates is given by

$$\mathbf{z} = T(x) = \begin{pmatrix} x_3 \\ x_7 \\ x_4 \\ x_5 \\ x_1 \\ x_2 \\ -x_5 g_1[6] + x_6 g_1[5] \end{pmatrix}. \tag{42}$$

Note that $g_1[5], g_1[6]$ are now functions of $\alpha = z_3$ only. Using the change of variables (42) and the feedback law (33)–(34), the equations of the system become

$$\dot{z}_1 = z_2, \quad \dot{z}_2 = w_1 \tag{43}$$

$$\dot{z}_3 = z_4, \quad \dot{z}_4 = w_2 \tag{44}$$

$$\dot{z}_5 = \left(\frac{z_7 + g_1[6]z_4}{g_1[5]}\right) \cos(z_1)$$

$$\dot{z}_6 = \left(\frac{z_7 + g_1[6]z_4}{g_1[5]}\right) \sin(z_1)$$

$$\dot{z}_7 = z_4 \left(-z_4 \frac{\partial g_1[6]}{\partial z_3} + \frac{\partial g_1[5]}{\partial z_3} \frac{z_7 + g_1[6]z_4}{g_1[5]}\right)$$

$$+ g_1[5] \left(f_2[2] - f_2[1]\frac{g_1[6]}{g_1[5]}\right) \tag{45}$$

where $f_2[1], f_2[2], f_2[3], g_1[5], g_1[6]$ are understood to be written in terms of $\mathbf{z}$. Note that inputs are explicitly absent from the last three equations, and they therefore represent the internal dynamics.

V. VELOCITY CONTROLLER DESIGN USING PARTIAL LINEARIZATION

The results from the sections above can be used to design a nonlinear controller which can track specified reference heading speed v and vehicle orientation θ; these are denoted as v_d and θ_d, respectively. The controller makes sure that $\alpha \in A_s = \{|\alpha| < \alpha_m < \pi/2\}$ for a given $\alpha_m > 0$. Note that this is a physically meaningful problem because, using these reference commands, one can safely follow a motion plan. The essential idea is to use the pitch angle α as a "gas pedal" for the vehicle and use it to accelerate and decelerate until the specified speed is attained.

The following should be noted.
1) $\alpha(t_0) \in A_s$ should be assured before starting the controller at time t_0.
2) Referring to (26) and (27), we see that $g_1[5] > 0, g_1[6] < 0$ if $\alpha \in (-\pi/2, \pi/2)$ which is its operating range. The limiting case is when the pendulum body pitches forward or backward such that it is horizontal. Thus, making sure that $\alpha(t) \in A_s, t > t_0$, ensures safe operation.

First, the dependence of the acceleration $\dot{v}$ on α is derived

$$v = x_6 = \left(\frac{z_7 + g_1[6]z_4}{g_1[5]}\right), \quad z_3 = \alpha, \quad z_4 = \dot{\alpha}, \quad z_1 = \theta. \tag{46}$$

Plugging these in the last of (45), we obtain

$$\dot{z}_7 + \dot{\alpha}^2 \frac{\partial g_1[6]}{\partial \alpha} \equiv \Gamma = (v\dot{\alpha})\frac{\partial g_1[5]}{\partial \alpha} + g_1[5]f_2[2] - g_1[6]f_2[1]. \tag{47}$$

Differentiating (46) and substituting expressions from (47), one obtains

$$\dot{v} = \frac{1}{g_1[5]}(\Gamma + g_1[6]w_2) - \frac{(v\dot{\alpha})}{g_1[5]} \frac{\partial g_1[5]}{\partial \alpha}$$

$$= \frac{1}{g_1[5]}(g_1[5]f_2[2] - f_2[1]g_1[6] + g_1[6]w_2). \tag{48}$$

Now the basic idea is to have $\theta = \theta_d, \dot{\theta} = 0$ and $\alpha = \alpha_r, \dot{\alpha} = 0$, where α_r is yet unspecified. This control is actually simple to achieve due to the linear structure in the θ system given by (43) and in the α system of (44). Having achieved this, in the steady state $\dot{\alpha} = 0, \dot{\theta} = 0$ and the acceleration expression from (48) can be written as

$$\dot{v}_{\text{ss}} = f_{\text{ss}}(\alpha_r) = \left[\frac{1}{g_1[5]}(g_1[5]f_{22}^\alpha - f_{21}^\alpha g_1[6])\right]_{\alpha = \alpha_r}. \tag{49}$$

Note that, in the steady state, $w_2 = 0$ because it is used to control only the α system and $\alpha = \alpha_r$. Expressions for f_{21}^α and f_{22}^α are given in the Appendix and are marked by underbraces. The function $f_{\text{ss}}(\alpha)$ is plotted in Fig. 2.

One observes that $f_{\text{ss}}(\alpha)$ is monotonic and odd in the range $\alpha \in (-\pi/2, \pi/2)$. Also, for a considerable range of α's near zero, the behavior is linear. We can now construct a two-layer controller: a higher level controller with slower dynamics for setting α_r and a lower level controller with much faster dynamics for tracking α_r and θ_d using controls w_2 and w_1, respectively. The lower level controller is easy to design due to the linear structure of (43) and (44).

A. Lower Level Controller C_l

One can choose

$$w_1 = -k_{qv}\dot{\theta} - k_q(\theta - \theta_d), \quad w_2 = -k_{av}\dot{\alpha} - k_a(\alpha - \alpha_r). \tag{50}$$

The gain constants $(k_{qv}, k_q, k_{av}, k_a)$ should be high enough to ensure subsecond convergence. To get the actual motor torques, one has to apply the reverse feedback laws $\mathbf{w} \rightarrow \mathbf{v} \rightarrow \tau/\mathbf{u}$. This controller tracks θ_d, α_r while taking $\dot{\theta}, \dot{\alpha}$ to 0 in steady state.

B. Higher Level Controller C_h

This controller C_h has slower dynamics and assumes that the lower level controller C_l is able to track its reference α_r "fast enough." C_h also has to make sure that $\alpha_r \in A_s$ for a given $\alpha_m \in (0, \pi/2)$. It has to then vary α_r to track the specified desired heading speed v_d. However, for $c_z = 0$, this approach cannot be used as α_r has no effect on the steady-state forward acceleration.

Consider the Lyapunov function

$$V_\Sigma = \frac{1}{2(\alpha_m^2 - \alpha_r^2)} + \frac{k_v(v_{\text{ss}} - v_d)^2}{2} \tag{51}$$

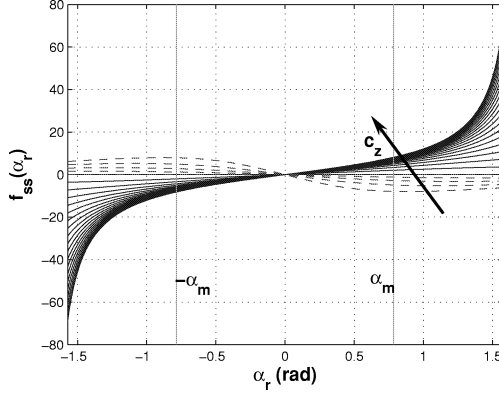Fig. 2. $f_{\mathrm{ss}}(\alpha_r)$ plotted for $\alpha_r \in (-\pi/2, \pi/2)$, for different values of c_z. Negative c_z curves are shown in dotted lines. The arrow denotes the direction of increase of c_z. c_z values vary from $-0.75R$ to $10R$, where R is the radius of the wheels. For $c_z = 0$, $f_{\mathrm{ss}}(\alpha_r) \equiv 0$ and α_r has no effect on the steady-state forward acceleration.

$$\dot{V}_\Sigma = \frac{\alpha_r \dot{\alpha}_r}{(\alpha_m^2 - \alpha_r^2)^2} + k_v(v_{\mathrm{ss}} - v_d)\dot{v}_{\mathrm{ss}}. \qquad (52)$$

Substituting (49) into (52), one gets

$$\dot{V}_\Sigma = \frac{\alpha_r \dot{\alpha}_r}{(\alpha_m^2 - \alpha_r^2)^2} + k_v(v_{\mathrm{ss}} - v_d)f_{\mathrm{ss}}. \qquad (53)$$

This suggests the control law

$$\dot{\alpha}_r = -k_r f_{\mathrm{ss}} - k_v \left(\alpha_m^2 - \alpha_r^2\right)^2 (v_{\mathrm{ss}} - v_d)\frac{f_{\mathrm{ss}}(\alpha_r)}{\alpha_r}. \qquad (54)$$

Note the following properties of f_{ss}, the first of which is due to the fact that the function is odd:

$$\alpha_r f_{\mathrm{ss}}(\alpha_r) > 0, \quad \alpha_r \neq 0 \qquad (55)$$

$$\lim_{\alpha_r \to 0} \frac{f_{\mathrm{ss}}(\alpha_r)}{\alpha_r} = \frac{M_b R c_z g}{M_b R^2 + 2M_w R^2 + c_z R M_b + 2I_{\mathrm{wa}}}. \qquad (56)$$

Substituting (54) into (53), one obtains

$$\dot{V}_\Sigma = -\frac{k_r \alpha_r f_{\mathrm{ss}}}{(\alpha_m^2 - \alpha_r^2)^2} \leq 0. \qquad (57)$$

On using LaSalle's invariant set theorem and properties (55) and (56), one deduces that the system converges to

$$\lim_{t \to \infty} \alpha_r = 0, \quad \dot{\alpha}_r = 0 \Rightarrow v_{\mathrm{ss}} = v_d. \qquad (58)$$

This can be seen by setting the control law defined by (54) to zero and putting α_r to zero. Also, as $\alpha_r(t_0) \in A_s$, and the Lyapunov function is nonincreasing under the control law, the reference pitch angle α_r cannot go out of A_s due to the barrier offered by the first term in V_Σ.

The dynamics of this controller can be slowed down by adjusting the gains k_r, k_v.

The stability proofs of these controllers apply in their respective time-scales only. Hence, one would like to make sure that the higher level controller is activated only when the lower level controller has converged. One approach to accomplish this would be to apply it in a discrete fashion every δt milliseconds, where δt is greater than the stabilization time for the lower level linear controller.

Another effective approach of making the dynamics of α_r slower than that of the actual pitch angle α is to multiply the right-hand side of (54) by $e^{-\hat{k}|\alpha|}, \hat{k} \gg 1$. The rationale of this is that, as long as the real pitch rate is high, $\dot{\alpha}_r$ remains small, i.e., α_r remains almost constant until the lower level controller catches up. Both approaches work,

TABLE I
SIMULATION PARAMETERS

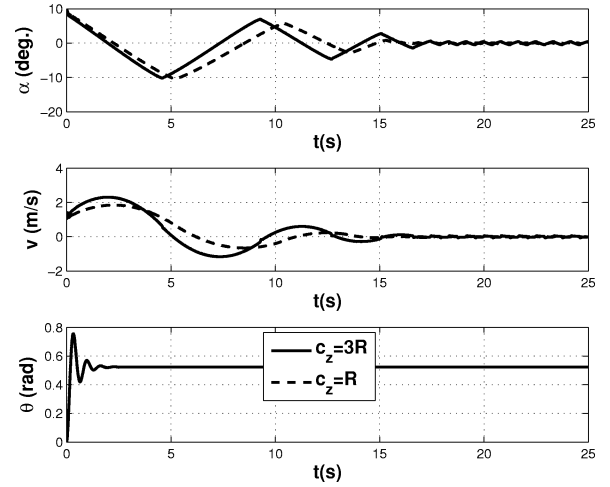| M_b	35.00	Kg
M_w	5	Kg
R	0.25	m
c_z	$R, 3R$	m
b	0.20	m
I_{xx}	2.1073	Kg m^2
I_{yy}	1.8229	Kg m^2
I_{zz}	0.6490	Kg m^2
I_{wa}	0.1563	Kg m^2
I_{wd}	0.0781	Kg m^2
α_m	$\pi/9, \pi/4$	rad
k_q	100	N/rad
k_{qv}	5	N/(rad/s)
k_a	1000	N/rad
k_{av}	50	N/(rad/s)
k_r	20	N/rad
k_v	$10/\alpha_m^4$	N/(rad/s)
$\hat{k}$	100	s/rad

Fig. 3. Comparison of responses to a stop command $v_d = 0, \theta_d = \pi/6 = 0.52$ for $c_z = R$ and $c_z = 3R$ with $\alpha_m = \pi/9 \equiv 20°$. The initial speed $v(t_0) = 1$ m/s and initial angles were $\theta(t_0) = 0, \alpha(t_0) = \pi/18 \equiv 10°$.

though we present simulation results of the second approach only because it automatically adjusts to any changes in the time-constant of the lower level controller.

Remark on Internal Dynamics: We can note from the internal dynamics (41) that ϕ_1 and ϕ_2 correspond to the x_o, y_o Cartesian coordinates, respectively. The third internal dynamics variable ϕ_3 is clearly a linear combination of the forward heading speed v and $\dot{\alpha}$, according to the third term of (41), where the scaling factors $g_1[5]$ and $g_1[6]$ are bounded functions of α. For the velocity controller, $\phi_1 = x_o, \phi_2 = y_o$ will not be bounded. This is to be expected because one is controlling velocity, not position. However, as v is bounded, because it is a controlled state, $\dot{x}_o, \dot{y}_o$ will also be bounded. Similarly, as both v and $\dot{\alpha}$ are controlled, ϕ_3, which is a linear combination, will remain bounded.

C. Simulation Results

For the simulations, the values taken are listed in Table I. Fig. 3 shows the response of a stop command $v_d = 0$ for nonzero high initial speed and pitch. In addition, the vehicle is commanded to stop at orientation $\theta_d = \pi/6$ rads. The responses for two values of c_z are
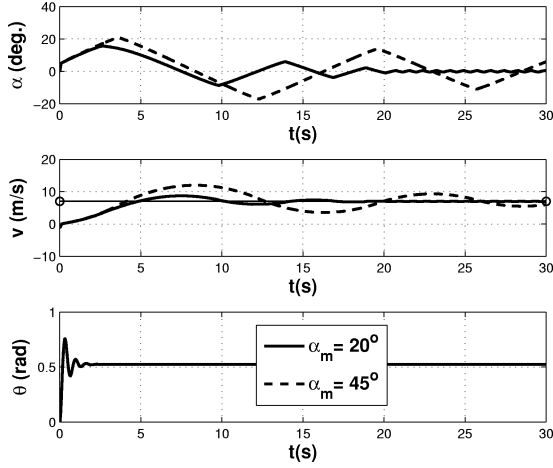
Fig. 4. Comparison of responses to a step command $v_d = 7$ m/s, $\theta_d = \pi/6 = 0.52$ for $\alpha_m = \pi/9 \equiv 20°$, and $\alpha_m = \pi/4 \equiv 45°$. The initial speed $v(t_0) = 0$ m/s and initial angles were $\theta(t_0) = 0$, $\alpha(t_0) = 0$.

compared. A higher c_z shows higher oscillation amplitudes in v before settling down. The controller was able to stop the vehicle in about 15 s. The simulation is for illustration only and, in a real system, the controller parameters should be adjusted to halt the system sooner for safety reasons.

Fig. 4 shows the result of specifying a step command for a high speed $v_d = 7$ m/s and $\theta_d = \pi/6$ rads from zero initial speed, pitch, and orientation for two different pitch-limits α_m. Note that the controller follows the limits rather conservatively. A higher α_m leads to quicker acceleration but also more oscillation in v and hence the settling time is increased.

VI. POSITION STABILIZATION CONTROL

In this section, a controller is designed to stabilize the coordinates of the point O (Fig. 1) (x_o, y_o) to the origin of $\mathcal{E}$ using smooth feedback control. The correct final orientation of the robot is not achieved using this control: however, this can be easily achieved by an in-place rotation using the linear subsystem (43) and the previously derived nonlinear feedback equations (33) and (23), once the desired position has been stabilized. The issue of stabilization of nonholonomic mobile robots has been studied extensively in the literature (see, e.g., [10] and [11]). A stabilization of a nonholonomic system in configuration space is usually not possible by a continuously differentiable, time-invariant state-feedback law, as pointed out by Brockett [12]. This applies to the system under study as it violates a necessary condition stated in Brockett's theorem. In this section, we take the approach of Astolfi [11], wherein a coordinate transform changes the continuous system to a discontinuous one, whereupon a continuous stabilizing state-feedback can be obtained. As in [11], a Cartesian-to-polar coordinate transform is used.

To stabilize to the origin of $\mathcal{E}$, polar coordinates are used as illustrated in Fig. 5. The configuration of the system and its time-derivative can now be expressed as

$$\mathbf{p} \equiv [\rho, \phi, \theta, \alpha]^T \tag{59}$$

$$\dot{\mathbf{p}} = \begin{pmatrix} 0 & \cos(\theta - \phi) & 0 \\ 0 & \sin(\theta - \phi)/\rho & 0 \\ 0 & 0 & 1 \\ 1 & 0 & 0 \end{pmatrix} \begin{pmatrix} \dot{\alpha} \\ v \\ \dot{\theta} \end{pmatrix} = \hat{S}(\mathbf{p})\boldsymbol{\nu}. \tag{60}$$

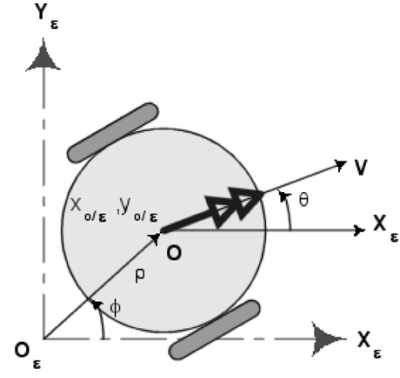$\boldsymbol{\nu}$ is as defined in (10).

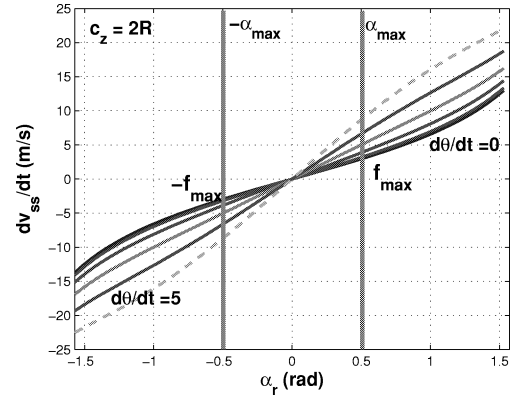Fig. 5. Top view of the vehicle at zero pitch, depicting the polar coordinates.

Fig. 6. Plot of $f_{ss}(\alpha_r, \dot{\theta})$ as a function of α_r for five different values of $\dot{\theta}$. The specified maximum allowable pitch angle α_{max} is marked by vertical lines. The intersection of these lines with the curve for $\dot{\theta} = 0$ is marked by the points $\pm f_{max}$.

A. Effect of Nonzero $\dot{\theta}$ on the Steady-State Heading Acceleration

In (49) and Fig. 2, the expression for the steady-state heading acceleration was found assuming that the angular speeds $\dot{\theta}$ and $\dot{\alpha}$ have already gone to zero. Now, we also consider the effect of nonzero $\dot{\theta}$. The pitch angular speed $\dot{\alpha}$ is still considered to be negligibly small, due to the selection of the control law. Now the expression in (49) is modified as

$$\dot{v}_{ss} = f_{ss}(\alpha_r, \dot{\theta}) = \left[\left(f_{22}^\alpha + f_{22}^{\dot{\theta}} \right) - \left(f_{21}^\alpha + f_{21}^{\dot{\theta}} \right) \frac{g_1[6]}{g_1[5]} \right]_{\alpha = \alpha_r}. \tag{61}$$

The expressions for $f_{21}^\alpha, f_{21}^{\dot{\theta}}, f_{22}^\alpha, f_{22}^{\dot{\theta}}$ are given in the Appendix and are marked with underbraces.

Equation (61) is plotted as a function of its arguments in Fig. 6. $f_{ss}(\alpha_r, \dot{\theta})$ is seen to *increase* in range as the absolute value of $\dot{\theta}$ increases. The function retains its *odd* property. These properties will be made use of in the controller design. The position controller is again a two-level controller. A higher level controller controls the θ system of (43) and determines a reference pitch angle $\alpha_r(t)$. This is then followed by a faster lower level controller which operates on the α system, (44).

B. Higher Level Controller

This controller is designed using two propositions.

Proposition 1: Let $V_\Sigma(\mathbf{p})$ be a potential field such that it is lower bounded and does not explicitly depend on α. On using a control law of the form

$$w_1 = -\frac{\partial V_\Sigma}{\partial \theta} - k_w \dot{\theta} \tag{62}$$

and setting the reference pitch angle α_r as the solution of

$$f_{ss}(\alpha_r, \dot{\theta}) = -\left[\frac{\partial V_\Sigma}{\partial \rho}\cos(\theta - \phi) + \frac{\partial V_\Sigma}{\partial \phi}\frac{\sin(\theta - \phi)}{\rho}\right] - k_v v. \quad (63)$$

$(k_w > 0, k_v > 0)$, the wheeled inverted pendulum mobile robot will converge to a manifold defined by

$$\mathcal{M} = \left\{\mathbf{p} : \hat{S}^T(\mathbf{p})\frac{\partial V_\Sigma}{\partial \mathbf{p}} = 0, \boldsymbol{\nu} = \mathbf{0}\right\}. \quad (64)$$

Proof: Consider a scalar function

$$V(\mathbf{p}, \boldsymbol{\nu}) = V_\Sigma(\mathbf{p}) + \frac{v^2}{2} + \frac{\dot{\theta}^2}{2} \quad (65)$$

where $V_\Sigma(\mathbf{p})$ is lower bounded as mentioned before. For this higher level controller, one assumes that $\dot{\alpha}$ is negligible, therefore $\dot{v} = \dot{v}_{ss} = f_{ss}$ and therefore (61) can be used. On differentiating V with respect to time and substituting (43) and (60), one gets

$$\dot{V}(\mathbf{p}, \boldsymbol{\nu}) = \left[\frac{\partial V_\Sigma}{\partial \mathbf{p}}\right]^T \dot{\mathbf{p}} + (0 \quad \dot{v} \quad \ddot{\theta})\boldsymbol{\nu} \quad (66)$$

$$= \boldsymbol{\nu}^T\left[\hat{S}^T(\mathbf{p})\frac{\partial V_\Sigma}{\partial \mathbf{p}} + \begin{pmatrix} 0 \\ f_{ss}(\alpha, \dot{\theta}) \\ w_1 \end{pmatrix}\right]. \quad (67)$$

As mentioned before, V_Σ is chosen not to have any explicit dependence on α. Equation (67) then can be expanded as

$$\dot{V} = v\left(\frac{\partial V_\Sigma}{\partial \rho}\cos(\theta - \phi) + \frac{\partial V_\Sigma}{\partial \phi}\frac{\sin(\theta - \phi)}{\rho} + f_{ss}(\alpha, \dot{\theta})\right)$$
$$+ \dot{\theta}\left(w_1 + \frac{\partial V_\Sigma}{\partial \theta}\right). \quad (68)$$

On substitution of the proposed control law (63) in the above, one gets

$$\dot{V} = -k_w\dot{\theta}^2 - k_v v^2 \leq 0. \quad (69)$$

V is lower bounded as V_Σ is assumed to be lower bounded. $\dot{V}$ has been shown to be negative semidefinite. Consider the system-state to lie in the set

$$\Omega = \{|\boldsymbol{\nu}| \in [\mathbf{0}, \infty); \alpha \in (-\pi/2, \pi/2);$$
$$\theta, \phi \in (-\pi, \pi); \rho \in [0, \infty)\}. \quad (70)$$

Using the invariant set theorem [9], the system will converge to

$$\frac{\partial V_\Sigma}{\partial \theta} = 0 \quad (71)$$

$$\frac{\partial V_\Sigma}{\partial \rho}\cos(\theta - \phi) + \frac{\partial V_\Sigma}{\partial \phi}\frac{\sin(\theta - \phi)}{\rho} = 0 \quad (72)$$

$$\dot{\theta} = 0, \quad v = 0, \quad f_{ss}(\alpha_r, \dot{\theta}) = 0 \Rightarrow \alpha_r = 0, \quad \dot{\alpha}_r = 0. \quad (73)$$

This can be seen by setting the control laws given by (63) and (62) to zero and substituting zeros for v and $\dot{\theta}$. Equation (72) gives an equilibrium invariant set which is the same as the set $\mathcal{M}$ in the proposition.∎

Now remains the task of finding a suitable V_Σ. Since $f_{ss}(\alpha_r, \dot{\theta} = 0)$ is bounded by f_{max} as shown in Fig. 6, V_Σ has to be such that the control law (63) is realizable. Also, one needs to make sure that the invariant set $\mathcal{M}$ consists of $\rho = 0$ so that the desired position stabilization to the origin is achieved.

Proposition 2: Consider the candidate function

$$V_\Sigma(\rho, \phi, \theta) = k_\Sigma \frac{\rho^2}{\sigma + \cos(\theta - \phi)}, \qquad \sigma > 1. \quad (74)$$

Then the requirements of Proposition 1 are satisfied and, additionally, the invariant set $\mathcal{M}$ consists of $\rho = 0, \alpha = 0, \boldsymbol{\nu} = \mathbf{0}$.

Proof: As $\rho^2 \geq 0$ and $|\cos(\theta - \phi)| \leq 1$, V_Σ is lower bounded by 0. Substituting (74) into (71), one obtains

$$k_\Sigma \frac{\rho^2 \sin(\theta - \phi)}{(\sigma + \cos(\theta - \phi))^2} = 0. \quad (75)$$

Substituting (74) into (72), one obtains

$$k_\Sigma\rho \frac{3\cos^2(\theta - \phi) + 2\sigma\cos(\theta - \phi) - 1}{(\sigma + \cos(\theta - \phi))^2} = 0. \quad (76)$$

Equation (75) is satisfied if either $\rho = 0$ or if $\theta - \phi = n\pi$.

1) If $\rho = 0$, (76) is also satisfied.
2) If $\theta - \phi = n\pi$, (76) is only satisfied if $\rho = 0$. This is because $3\cos^2(\theta - \phi) + 2\sigma\cos(\theta - \phi) - 1 \neq 0$ for $(\theta - \phi) = n\pi$, if $\sigma > 1$.

In any case, our objective of converging to $\rho = 0$ is satisfied. Furthermore, (63) now amounts to finding a value of α_r such that

$$f_{ss}(\alpha_r, \dot{\theta}) = -k_\Sigma\rho \frac{3\xi^2 + 2\sigma\xi - 1}{(\sigma + \xi)^2} - k_v v,$$
$$\xi \equiv \cos(\theta - \phi) \in [-1, 1].$$

Once a maximum allowed pitch α_{max} is decided, Fig. 6 shows that $|f_{ss}(\alpha_r, \dot{\theta} = 0)| \leq f_{max}$. Due to the asymptotic convergence of ρ to 0, one expects it to be a decaying function of time, with some initial oscillations due to nonzero initial velocities. One can therefore decide on a value $\rho_m > \rho(t_0)$ such that $\rho_m > \rho(t), t > t_0$.

Equation (77) always has a feasible $|\alpha_r| \leq \alpha_{max}$ as a solution for $v = 0$, if

$$f_{max} \geq \Xi_m, \quad (77)$$

$$\Xi_m \equiv \max_{\xi \in [-1, 1]}\left|k_\Sigma\rho_m \frac{3\xi^2 + 2\sigma\xi - 1}{(\sigma + \xi)^2}\right|. \quad (78)$$

It can be shown that this maximum value Ξ_m occurs at the boundary $(\xi = \pm 1)$ or at $\xi_m = -(\sigma^2 + 1)/2\sigma$ if $|\xi_m| \leq 1$. For a given σ, this maximum value can be precomputed, e.g., for $\sigma = 2, \Xi_m = 2\rho_m$. We can now choose the gain $K_\Sigma \geq f_{max}/\Xi_m$ to always ensure a feasible solution $|\alpha_r| \leq \alpha_{max}$ for $v = 0$. f_{max} was computed assuming $\dot{\theta} = 0$. For nonzero $\dot{\theta}$, Fig. 6 shows that the available range of $|f_{ss}|$ is actually *higher* and, therefore, a feasible α_r can still be found.

The leeway between Ξ_m and the actual value of the function on the right-hand side of (78) can be used to compute a feasible value of k_v for nonzero heading speeds. This means that the value of $k_v \geq 0$ can potentially change from its nominal positive value if the nominal value is not feasible at a given time-instant. Note that $k_v = 0$ is guaranteed to be feasible so an iterative reduction of k_v in case of infeasibility is bound to find a solution for any value of v. ∎

C. Lower Level Controller

This controller is designed to give a subsecond convergence to the desired α_r set by the higher level controller. Using the linear subsystem (44), this can be achieved by

$$w_2 = -k_{av}\dot{\alpha} - k_a(\alpha - \alpha_r). \quad (79)$$

The gain constants (k_{av}, k_a) should be sufficiently high to ensure subsecond convergence. To get the actual motor torques one has to apply the reverse nonlinear feedback laws $\mathbf{w} \rightarrow \mathbf{v} \rightarrow \tau/\mathbf{u}$.

Remark on Internal Dynamics: Clearly, as the controller guarantees asymptotic convergence of the polar coordinate $\rho = \sqrt{x_o^2 + y_o^2}$ to 0,

$$\mathbf{f_2[1]}(\mathbf{x}) = \underbrace{\frac{\sin(2\alpha)\dot{\theta}^2 \bar{H}}{D_\alpha}}_{f_{21}^{\dot{\theta}}} + 1/2\frac{M_b^2 c_z^2 R^2 \sin(2\alpha)(\dot{\alpha})^2}{D_\alpha} + \underbrace{1/2\frac{\left(-2M_b^2 R^2 c_z - 4I_{\mathrm{wa}}M_b c_z - 4M_w R^2 M_b c_z\right) g\sin(\alpha)}{D_\alpha}}_{f_{21}^{\alpha}} \tag{87}$$

$$\mathbf{f_2[2]}(\mathbf{x}) = \underbrace{K_\alpha \dot{\theta}^2}_{f_{22}^{\dot{\theta}}} + \underbrace{1/2\frac{M_b^2 c_z^2 R^2 g \sin(2\alpha)}{D_\alpha}}_{f_{22}^{\alpha}} + 1/4\frac{\left(-4I_{yy}M_b R^2 c_z - 4R^2 M_b^2 c_z^3\right)\sin(\alpha)(\dot{\alpha})^2}{D_\alpha} \tag{88}$$

TABLE II
MODIFIED/ADDITIONAL SIMULATION PARAMETERS

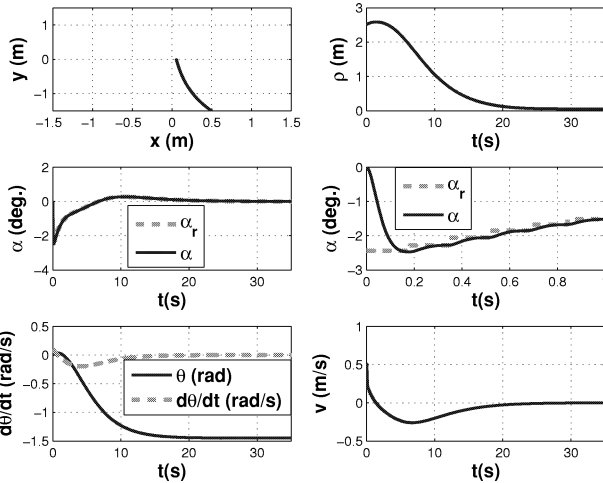|		
c_z	$2R$	m
k_a	828.42	N/rad
k_{av}	46.05	N/(rad/s)
k_w	0.2	N/(rad/s)
k_v nominal	0.6	N/(m/s)
ϵ	0.001	rad/s
$\alpha_{\max}$	$\pi/36$	rad (5°)
$\alpha(t_0)$	0	rad
$\dot{\alpha}(t_0)$	0	rad/s
$v(t_0)$	0.25	m/s
$\theta(t_0)$	0	rad
$\phi(t_0)$	$-\pi/3$	rad
$\rho(t_0)$	2.5	m
$\dot{\theta}(t_0)$	0.1	rad/s

Fig. 7. Simulation plots for 35 s. The second figure in second row shows a zoomed-in view for comparing α_r and α. ρ and α, v, and $\dot{\theta}$ are seen to be converging to zero.

both $\phi_1 = x_o$ and $\phi_2 = y_o$ converge to 0. Similarly, as all of the speeds approach 0 due to asymptotic stability, ϕ_3 also approaches 0 asymptotically.

D. Simulation Results

The higher level controller is conditionally executed only when $|\dot{\alpha}| \leq \epsilon$, where $\epsilon \ll 1$. This ensures that the lower level controller has sufficiently converged. Most simulation parameters are the same as in Table I. Modified and additional parameters are given in Table II. Fig. 7 show the controllers at work. They take the vehicle from an offset of $\rho(0) = 2.5$ and, with some arbitrarily given initial orientation, heading, and turning speeds, to the origin at rest. During this motion, the vehicle pitch motion is restricted to $\pm 5^\circ$.

VII. CONCLUSION

The main contributions of this letter are as follows: 1) complete derivation of the dynamic equations of a wheeled inverted pendulum in terms of physical variables useful for motion planning and control; 2) study of the system's controllability properties and maximum relative degree and derivation of a partial feedback linearized form; 3) derivation of a two-level velocity controller which makes use of this partial feedback linearized form; and 4) derivation of a novel stabilizing position controller. Simulations with realistic data show that this approach is effective. Further work needs to be done to make the controller design robust with respect to parameter uncertainties.

APPENDIX

Detailed expressions from Section II are shown as follows, with (87) and (88) shown at the top of the page.

$$\begin{aligned}
D_\alpha \equiv\ & M_b^2 \cos^2(\alpha) c_z^2 R^2 \\
& + \left(\left(-M_b^2 - 2M_w M_b\right) c_z^2 - 2I_{yy}M_w - I_{yy}M_b\right) R^2 \\
& - 2M_b c_z^2 I_{\mathrm{wa}} - 2I_{yy}I_{\mathrm{wa}}
\end{aligned} \tag{80}$$

$$\begin{aligned}
G_\alpha \equiv\ & \left(-M_b c_z^2 + I_{zz} - I_{xx}\right) R^2 \cos^2(\alpha) \\
& + \left(M_b c_z^2 + I_{xx} + 2I_{\mathrm{wd}} + 2b^2 M_w\right) R^2 + 2b^2 I_{\mathrm{wa}}
\end{aligned} \tag{81}$$

$$\mathbf{g}(\mathbf{x}) = [\mathbf{g_1}(\mathbf{x}), \mathbf{g_2}(\mathbf{x})] \tag{82}$$

$$\mathbf{g_1}(\mathbf{x}) = \begin{pmatrix} \mathbf{0}_{4\times 1} \\ \frac{M_b R^2 + 2M_w R^2 + 2I_{\mathrm{wa}} + M_b \cos(\alpha)c_z R}{D_\alpha} \\ -\frac{R\left(M_b \cos(\alpha)c_z R + I_{yy} + M_b c_z^2\right)}{D_\alpha} \\ \frac{Rb}{G_\alpha} \end{pmatrix} \tag{83}$$

$$\mathbf{g_2}(\mathbf{x}) = \begin{pmatrix} \mathbf{0}_{4\times 1} \\ \frac{M_b R^2 + 2M_w R^2 + 2I_{\mathrm{wa}} + M_b \cos(\alpha)c_z R}{D_\alpha} \\ -\frac{R\left(M_b \cos(\alpha)c_z R + I_{yy} + M_b c_z^2\right)}{D_\alpha} \\ -\frac{Rb}{G_\alpha} \end{pmatrix} \tag{84}$$

$$\begin{aligned}
\bar{H} \equiv\ & 1/2 M_b R^2 I_{zz} + I_{\mathrm{wa}}I_{zz} - M_w R^2 I_{xx} \\
& - I_{\mathrm{wa}}I_{xx} - M_b c_z^2 M_w R^2 - M_b c_z^2 I_{\mathrm{wa}} \\
& - 1/2 M_b R^2 I_{xx} + M_w R^2 I_{zz}
\end{aligned} \tag{85}$$

$$\begin{aligned}
K_\alpha(4D_\alpha) \equiv\ & \left(-4I_{yy}M_b R^2 c_z - 3R^2 M_b^2 c_z^3 \right. \\
& \left. + M_b R^2 c_z (I_{xx} - I_{zz})\right)\sin(\alpha) \\
& + \left(M_b R^2 c_z (I_{xx} - I_{zz}) \right. \\
& \left. + R^2 M_b^2 c_z^3\right)\sin(3\alpha)
\end{aligned} \tag{86}$$

$$\begin{aligned}
\mathbf{f_2[3]}(\mathbf{x}) =\ & \frac{\left(-(I_{xx} - I_{zz})R^2 - M_b c_z^2 R^2\right)\sin(2\alpha)\dot{\alpha}\dot{\theta}}{G_\alpha} \\
& - \frac{\sin(\alpha)R^2 M_b c_z v\dot{\theta}}{G_\alpha}
\end{aligned} \tag{89}$$

REFERENCES

[1] R. Marino, "On the largest feedback linearizable subsystem," *Syst. Control Lett.*, vol. 6, pp. 345–351, 1986.

[2] H. Nijmeijer and A. J. van der Schaft, *Nonlinear Dynamical Control Systems*. Berlin, Germany: Springer-Verlag, 1990.

[3] A. Salerno and J. Angeles, "On the nonlinear controllability of a quasiholonomic mobile robot," in *Proc. IEEE ICRA*, Taiwan, 2003, pp. 3379–3384.

[4] ——, "The control of semi-autonomous two-wheeled robots undergoing large payload-variations," in *Proc. IEEE ICRA*, New Orleans, LA, Apr. 2004, pp. 1740–1745.

[5] Y.-S. Ha and S. Yuta, "Trajectory tracking control for navigation of the inverse pendulum type self-contained mobile robot," *Robot. Autonom. Syst.*, vol. 17, pp. 65–80, 1996.

[6] M. Baloh and M. Parent, "Modeling and model verification of an intelligent self-balancing two-wheeled vehicle for an autonomous urban transportation system," in *Proc. Conf. Comp. Intelligence, Robot. Autonom. Syst.*, Singapore, Dec. 2003.

[7] Segway Human Transporter (2004). [Online]. Available: http://www.segway.com

[8] F. Grasser, A. D'Arrigo, S. Colombi, and A. Rufer, "Joe: A mobile, inverted pendulum," *IEEE Trans. Ind. Electron.*, vol. 49, no. 1, pp. 107–114, Feb. 2002.

[9] J.-J. Slotine and W. Li, *Applied Nonlinear Control*. Englewood Cliffs, NJ: Prentice-Hall, 1991.

[10] A. M. Bloch, M. Reyhanoglu, and N. H. McClamroch, "Control and stabilization of nonholonomic dynamic systems," *IEEE Trans. Automat. Control*, vol. 37, no. 11, pp. 1756–1757, Nov. 1992.

[11] A. Astolfi, "Asymptotic stabilization of nonholonomic systems with discontinuous control," Ph.D. dissertation, Swiss Federal Inst. of Technol., Zurich, Switzerland, 1996.

[12] R. W. Brockett *et al.*, "Asymptotic stability and feedback stabilization," in *Differential Geometry Control Theory*, R. W. Brockett *et al.*, Eds. Boston, MA: Birkhäuser, 1983, vol. 27. Progress in Mathematics.

[13] I. Fantoni, R. Lozano, and M. W. Spong, "Energy based control of the pendubot," *IEEE Trans. Automat. Control*, vol. 45, no. 4, pp. 725–729, Apr. 2000.

[14] A. Blankespoor and R. Roemer, "Experimental verification of the dynamic model for a quarter size self-balancing wheelchair," in *Proc. ACC*, Boston, MA, Jun. 2004, pp. 488–492.

Turning Behavior Modeling for the Heading Control of an Articulated Micro-Tunneling Robot

Koichi Yoshida and Tadashi Haibara

Abstract—The performance of a microtunneling robot to be driven along a projected line is strongly dependent on the skill of the operator. The heading control of the driving machine is the key to achieving an autonomous navigation system. This paper presents a design scheme for models to describe driving machine turning behavior of an articulated micto-tunneling robot. Two types of model are introduced based on the offline analysis of a driving data obtained at an actual construction site: a model with a head motion constraint and a model with a rear end motion constraint. Simulation results are provided, in which a Kalman filter is applied to the models to verify the online state estimation performance obtained using the driving data, and the two models are compared in terms of their estimation and prediction errors.

Index Terms—Kalman filter, microtunneling robot, modeling, motion constraint.

I. INTRODUCTION

As an alternative to the more restrictive open-cut method, the micro tunneling technology is receiving attention from the aspects of economy and environmental conditions, and there are demands to increase its range of applications and accuracy. Representative micro tunneling technologies include the press-insertion method, the auger method and the balance method. These are selected depending on the line shape and the type of soil in the section to be tunneled, as well as for such reasons as economy, and low pollution. The Acemole DL method, which is a kind of slurry and earth pressure balance method, can be used with a variety of excavation cutter heads, enabling it to cope with a wide range of soil, from ordinary soil to ground containing pebbles and rubble stones, and can also be used for tunneling over long distances [1], [2]. In addition, new operation systems aimed at reducing the initial installation costs of foundation facilities have been developed [3], [5].

Design schemes for the control system of the tunneling robot have been studied with a view to developing autonomous navigation systems for the highly accurate, automatic direction control of discharge-type microtunneling machines (Acemole DL method) [4], [9]. Previously, the performance of this type of tunneling robot was strongly dependent on the skill of the operator. The tunneling robot is equipped with various sensors to locate its driving machine at the tunneling end with respect to a projected (reference) line. However, the regular measurement process (detailed in Section II) has insufficient accuracy and noise tolerance, especially for the detection of the horizontal position and the orientation of the driving machine. This is because of the lack of a direct sensing device to provide this information.

This paper discusses a modeling method that describes the horizontal turning behavior of the driving machine, and an online estimation scheme for the horizontal position and orientation as well as turning characteristic parameters. In this modeling approach, we show that if the turning curvature of each part and the moving direction of a portion (e.g., the head tip or rear end) on the driving machine are given,